Carbon 232 (2025) 119796

Contents lists available at ScienceDirect

Carbon

journal homepage: www.elsevier.com/locate/carbon

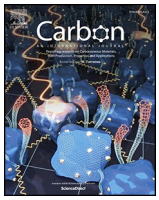

Interrogating the photoluminescent properties of carbon dots using quantitative ^{13}C NMR combined with systematic photobleaching

Leslie R. Sigmon [a], Jonathan Catazaro [a], Mohammed Abdel-Rahman [a], Casey Smith [a], Carsten Prasse [b], D. Howard Fairbrother [a,*]

[a] Department of Chemistry, Johns Hopkins University, Baltimore, MD, 21218, USA
[b] Department of Environmental Health and Engineering, Johns Hopkins University, Baltimore, MD, 21218, USA

A B S T R A C T

In this work, molecular-level events accompanying the photobleaching of carbon dots (CDs) synthesized from ethylenediamine and citric acid (CACDs) were identified using solution-phase NMR. By combining quantitative ^{13}C NMR data with fluorescence measurements we show that this new approach is capable of identifying not only molecular fluorophores in CACDs, but also their contribution to the overall CACD fluorescence and their relative photostability. Specifically, imidazo[1,2-a]pyridine-7-carboxylic acid (IPCA) is found to be the dominant (84 %) species responsible for fluorescence in CACDs along with a second undetermined source, most likely associated with the aromatic core which is significantly (approximately 20 times) more photostable than IPCA. The presence of these two fluorescent species with different photostabilities rationalizes not only the photobleaching kinetics but also the evolution of the fluorescence spectrum during photobleaching Diffusion-ordered spectroscopy (DOSY) also reveals that all of the IPCA molecules are trapped within or covalently bound to the CACD, but are not present as isolated molecules freely rotating in solution. Singlet oxygen is confirmed as a key ROS responsible for photobleaching, with prototypical photoproducts identified from mass spectrometry studies of citrazinic acid. Quantitative ^{13}C NMR of CACDs is possible because their extremely high colloidal stability enables high concentrations (667 mg/mL) to remain stable in solution. The approach described in this study could be extended to identify the structure of chromophores in other CDs and interrogate molecular level processes that accompany CD sensing.

1. Introduction

Carbon dots (CDs) are fluorescent carbon nanomaterials with optical properties that have high quantum yields (QY) and tunable fluorescence [1,2]. CDs are often considered to be an environmentally-friendly substitute for quantum dots (QDs), because CDs can be used in many of the same optoelectronic applications [3], like bioimaging [4–6], sensing [7–11], energy conversion [12], lighting [13–15], and displays [16,17], but CDs can be prepared using earth abundant elements and from an array of sustainable materials such as agricultural waste [18–21] and discarded plastic bags [22,23]. CDs can be made using either top-down or bottom-up methods, but bottom-up methods have attracted particular attention due to their facile and inexpensive syntheses [24,25]. CDs produced this way can exhibit high quantum yields [9,26], excellent water solubility and biocompatibility [1,27], and a broad range of emission wavelengths [10,28–30], with or without excitation-dependence [31], depending on the exact synthetic strategy. The multitude of precursors, preparation conditions, and post-synthetic treatments available to prepare CDs [32–35] results in a highly diverse range of materials with varied applications [36].

The origin of CD photoluminescence remains controversial for many CD types [24,37], with competing hypotheses attributing CD fluorescence to core, surface, or molecular states [3,37–42]. Quantum confinement-derived fluorescence has been observed in CDs with a high proportion of conjugated π-domains, and has been proposed as the main fluorescence source for top-down synthesized CDs often referred to as graphene QDs [37,38,43,44]. Surface defect fluorescence, most commonly found in bottom-up synthesized CDs with excitation-dependent fluorescence, is caused by energy transfer between the carbon core and surface functional groups which is influenced by defects and degree of oxidation [37,38,40,43,45]. CDs synthesized from citric acid and small organic precursors that typically contain amines usually exhibit high excitation-independent QYs, and the origin of photoluminescence is often attributed wholly to, or in part to pyridone-derived molecular fluorophores [31,32,39,44,46–52]. However, when citric acid is not used as a precursor different molecular fluorophores can be formed, depending upon the structure and properties of the precursor and reaction conditions.[53-58] For example, CDs with different band gaps have been prepared by pyrolysis of m-hydroxybenzaldehyde in different acid-base conditions [53].

* Corresponding author.
E-mail address: howardf@jhu.edu (D.H. Fairbrother).

https://doi.org/10.1016/j.carbon.2024.119796
Received 20 March 2024; Received in revised form 12 October 2024; Accepted 1 November 2024
Available online 2 November 2024

Regardless of the synthetic procedure, to determine these molecular fluorophores, researchers typically purify CDs using dialysis tubing, and characterize the fluorescent solution separated from CDs present outside of the tubing, using a variety of techniques such as liquid chromatography mass spectrometry (LC-MS) and nuclear magnetic resonance (NMR). Using this approach, Song et al. [59] synthesized CDs from citric acid and ethylenediamine, further purified and characterized the fluorescent dialysate using LC-MS and NMR, and identified imidazo[1,2-a] pyridine-7-carboxylic acid (IPCA) as the source of the blue-green fluorescence. Shi et al. [60] synthesized CDs using citric acid and L-cysteine, characterized the dialysate with MS, NMR, and thermogravimetric analysis (TGA), and discovered 5-oxo-3,5-dihydro-2H-thiazolo [3,2-a] pyridine-3,7-dicarboxylic acid (TPDCA) and 5-oxo-3,5-dihydro-2H-thiazolo [3,2-a] pyridine-7-carboxylic acid (TPCA) as a molecular source of blue fluorescence. Similarly, Liu et al. [61] used LC-MS and NMR to identify 1-(2-aminoethyl)-5-oxo-1,2,3,5-tetrahydroimidazo[1,2-a]-pyridine-7-carboxylic acid (AEIOP) in dialysate from CDs made using citric acid and diethylenetriamine as precursors, and Kasprzyk et al. [50] used LC-MS and NMR to determine citrazinic acid (CZA) and 4-hydroxy-1H-pyrrolo[3,4-*c*]pyridine-1,3,6(2H,5H)-trione (HPPT) as the sources of blue and green emission, respectively, in dialysate separated from CDs synthesized using citric acid and urea [31,34,62–64].

Photostability is another aspect of CDs that varies based on synthetic methods [47]. In the early literature, CDs were described as being highly resistant to photobleaching [29,30,46,47], the permanent loss of fluorescence due to chemical alteration of the fluorophore following periods of high intensity or prolonged irradiation [65]. The excellent photostability of CDs was considered to be a major advantage over other photoluminescent species, like fluorescent proteins or organic dyes [66]. However, more recent studies have shown that CDs are susceptible to photobleaching, depending on their structural characteristics. In general, more highly carbonized, lower QY CDs are more photostable than CDs synthesized by bottom-up methods which exhibit higher QYs and are typically assumed to contain molecular fluorophores [46,47,67]. Several studies have proposed that photobleaching occurs through a process of photooxidation, since deoxygenating solutions by purging with inert gases or encapsulating CDs within a polymer can greatly reduce photobleaching rates [68,69]. The chemical changes that happen within a CD during photobleaching have been explored by only a few studies; using attenuated total reflectance Fourier-transform infrared (ATR-FTIR) and Raman spectroscopy, Wang et al. [69] found evidence that photobleaching caused oxidation of C bonds, reduction in the overall number of surface functional groups, and a decrease in the nitrogen content of CDs. This is in contrast to results from our group that showed no significant changes to the CD structure or elemental makeup beyond the obvious loss of fluorescence [68].

In principle, studying the mechanism and kinetics of photobleaching can provide a route to gain deeper insight into CD structure and optical properties [47,70]. Indeed, the kinetics and dynamics of photobleaching in several types of CDs have been studied. Longo et al. [47] prepared CDs from citric acid and urea and found that when laser (355 nm or 266 nm) irradiated, the photobleaching kinetics were best fit to a stretched exponential function. This was taken as evidence for molecular fluorophores having photostabilities that were dependent upon their local environments. This and other observations by Longo et al. [47], including partial recovery of fluorescence after irradiation, led them to propose that CD fluorophores are weakly bound to the CD surface and are in dynamic equilibrium with identical free molecules in solution. Terracina et al. [70] synthesized CDs with a range of emission wavelengths from citric acid and a variety of amine-containing precursors, including trisaminomethane, urea, and hexadecylamine, and used a stretched-exponential kinetic model to support the idea of interactions between fluorophores and carbonaceous CD cores. However, Terracina et al. [70] propose that molecular fluorophores are strictly incorporated into the CD structure or bound on the CD surface and not in equilibrium with free molecules. In these photobleaching experiments using laser irradiation, Terracina et al. found no changes in the shape of CD emission profiles after irradiation, aside from reduced intensity, leading to their conclusion that the fluorescence arises entirely from a single molecular fluorophore in each of the CDs studied.

While these photobleaching studies have provided valuable insights into the photobleaching of CDs they do not provide direct spectroscopic information on the molecular processes that accompany photobleaching, an approach that in principle could directly identify the species responsible for CD fluorescence. In this regard, solution-phase NMR spectroscopy has the molecular specificity to answer many of the questions related to the structure, fluorescence and properties of CDs. Thus, NMR characterization on separated fractions of fluorescent material before or after CD purification is increasingly common and has led to several important insights into the identity of CD fluorophores [28,50,59,71–73]. Solution-phase NMR can be used for structural insight, for example, to characterize CD surface functionalization with organic ligands [74–77] and can be a simple way to determine the relative size of CDs [78–80]. Despite this potential utility, NMR of whole CDs is typically only used for routine 1D and sometimes 2D characterization, and often only to compare CD products to starting materials as evidence of a successful synthesis or purification [9,27,60,80–87]. Very rarely are NMR spectra in the literature used for quantitative analysis beyond basic identification of major groups of peaks, most likely because many published NMR spectra of whole CDs, especially ^{13}C, suffer from poor signal-to-noise ratios, with many spectroscopic features not discernible above the baseline [18,27,78,81].

In this work, molecular-level events that accompany photobleaching of CDs synthesized from ethylenediamine and citric acid (CACDs) and systematically irradiated with 350 nm light have been identified using solution phase NMR. By combining NMR data with fluorescence measurements obtained from photoluminescence spectroscopy we show that this new approach is capable of identifying not only the molecular fluorophores in CDs but is also able to directly quantify their contribution to the overall CD fluorescence as well as their photostability. Photobleaching kinetics data are complemented by studies conducted with a singlet oxygen radical scavenger, cysteine [88], as well as the use of citrazinic acid as a model fluorophore to identify potential photoproducts. One of the key innovations in the present study derives from the recognition that high concentrations of CDs (>600 mg/mL) can remain colloidally stable, opening up the opportunity to use quantitative ^{13}C NMR as a detailed structural probe of CDs and their transformations under the influence of external stimuli such as light.

2. Experimental

2.1. CD synthesis

Materials: Citric acid, ethylenediamine, citrazinic acid, deuterium oxide (D_2O), dimethyl sulfoxide-d6 (DMSO-d_6), L-cysteine, potassium tris(oxalato)ferrate(III) trihydrate, o-phenanthroline, acetate buffer solution (pH 3.5), and 3-(Trimethylsilyl)propionic −2,2,3,3-d_4 acid sodium salt (TMSP-d_4) were purchased from Sigma-Aldrich and used without further purification.

Synthesis: Citric acid carbon dots (CACDs) were synthesized via a previously described bottom-up microwave-assisted pyrolysis method [27,68]. In a beaker, 2 mL of 4 M citric acid and 540 μL of ethylenediamine were combined. Following the spontaneous reaction, the mixture was cooled to room temperature, then heated in a domestic microwave oven at 700 W for 2 min. Approximately 10 mL of deionized water was added to the solid product and the mixture was magnetically stirred until completely dissolved. The mixture was dialyzed against deionized water for 24 h using 0.1–0.5 kDa pore size dialysis tubing (Repligen, Waltham, MA, USA). Finally, the solution was dried in an oven at 60 °C until all water was evaporated.

2.2. CD characterization

ATR-FTIR: Attenuated total reflectance Fourier-transform infrared (ATR-FTIR) spectra were obtained using a Nicolet iS5 spectrometer (Thermo Fisher, Waltham, MA, USA) with an iD5 ATR attachment and a scan range of 4000-525 cm^{-1} with 32 scans at 0.964 cm^{-1} resolution.

Elemental analysis: Elemental analysis was conducted using an Exeter Analytical CE 440 CHN/O/S Elemental Analyzer (North Chelmsford, MA, USA).

Quantum Yield: The CACD quantum yield (QY) was measured using the relative approach described by Williams et al. [89], using quinine sulfate in 0.1 M H_2SO_4 as a reference, which has a known QY of 54.6 % [90]. In brief, CACD and the reference were dispersed in ultrapure water and 0.1 M H_2SO_4, respectively, and the concentration adjusted so that the absorbance at 350 nm (the peak of CACD absorbance - see Fig. S1) was 0.1 or lower to avoid inner filter effects. Fluorescence measurements were then taken using an excitation and emission slit width of 1 nm, with an excitation wavelength of 350 nm. Equation (1) was then used to determine the QY of the CACDs (QY_{CACD}):

$$QY_{CACD} = QY_{ref}\frac{A_{ref}\ F_{CACD}\ \eta^2_{CACD}}{A_{CACD}\ F_{ref}\ \eta^2_{ref}} \quad (1)$$

where QY is the quantum yield (%), A is the absorbance of the sample at 350 nm, F is the integral of the fluorescence emission scan, and η is the refractive index of the solvent. Using this analysis, QY values for CACDs synthesized as part of this study ranged from 47 to 54 %, typical of values reported in the literature [27,91].

Surface Charge: The zeta potential of CACDs was determined to be -10.6 ± 1.5 mV using a Malvern Zetasizer Nano, typical of the values reported for CDs synthesized using citric acid and small nitrogen-containing precursors such as ethylenediamine and urea [92].

NMR sample preparation: All NMR samples were made with a ratio of 400 mg CACDs to 600 μL deuterium oxide (D_2O) and prepared as follows. At least 350 mg of CACDs were weighed and placed in a 50 mL centrifuge tube and a proportionate amount of D_2O was added. The tubes were then sonicated in a Branson 1510 ultrasonicator bath (Danbury, CT) at 70 W for at least 1 h to completely disperse CACDs. This solution was then pipetted into a 5 mm O.D. diameter NMR tube (Wilmad-Labglass, Vineland, NJ, USA) and allowed to settle for at least 15 min.

NMR: Prior to conducting any other NMR measurements, the T_1 relaxation time of CACDs was determined by an inversion recovery pulse sequence and data fitting in Topspin (Bruker, Billerica, MA, USA). In order to ensure that all NMR spectra were quantitative, a relaxation delay of 10 s was used for all subsequent NMR measurements, which was at least 5x more than the longest determined T_1 value. ^1H and ^{13}C NMR spectra were obtained for the non-irradiated CACD sample and all photobleached CACD samples. Heteronuclear single quantum coherence (HSQC) and heteronuclear multiple bond correlation (HMBC) spectra were obtained for the non-irradiated and the 2-h photobleached CACD samples using standard Bruker pulse sequences. ^1H and ^{13}C NMR measurements as well as HSQC and HMBC were conducted using a 400 MHz NMR (Bruker UltraShield, Billerica, MA) at 25 °C. NMR spectra were analyzed with Topspin and MestReNova (Mestrelab Research, Santiago de Compostela, Spain).

Quantitative NMR with TMSP: Quantitation of ^{13}C and ^1H spectra were determined using 40 μM 3-(trimethylsilyl)propionic-d4 acid (TMSP) as an external reference. Nonspecific binding of TMSP to the CDs precluded its use as an internal standard. Quantification was achieved by acquiring a ^{13}C or ^1H spectrum on TMSP immediately after the CD acquisition, with the exact same experimental parameters, and a subsequent summation of the spectra.

CACD Fluorescence: Photoluminescence (PL) spectra were obtained using a Thermo Scientific Lumina fluorescence spectrometer (Waltham, MA, USA). An excitation wavelength of 350 nm was used, and emission spectra were recorded with a 0.1 nm interval from 360 to 650 nm, with 2.5 nm excitation and emission slit widths, a photomultiplier tube voltage of 700 V, and a 20 ms integration time. In order to avoid interference from inner filter effects, all CACD solutions used in PL measurements were 15 mg/L, at which concentration the absorbance at the characteristic peak circa 350 nm is ≤ 0.1, as measured by a Thermo Scientific Evolution 220 UV–Visible spectrometer (Waltham, MA, USA). A 1-cm path length quartz cuvette was used for all PL and UV–Vis measurements (Thorlabs, Newton, NJ, USA).

2.3. CACD photobleaching

Photobleached CACDs for NMR and PL experiments: To prepare photobleached CACDs for NMR and PL experiments, 500 mg CACDs were added to 2 L deionized H_2O, then irradiated with 350 nm light using a Rayonet photoreactor (Southern New England Ultraviolet Company, Branford, CT) equipped with 16 bulbs. The irradiated solution was then dried in an oven at 60 °C until all water was evaporated. Approximately 20 mg of the 400 mg of oven-dried CACDs were used for PL measurements, and the remainder used for NMR; mixtures of CACDs exposed to varying irradiation times were also studied. The approach of measuring PL spectra of photobleached CACDs after they had been reconstituted as powders ensured that PL and NMR data could be directly compared on the same photobleached CACDs. After completion of NMR measurements, the solution was extracted from the NMR tube and dried overnight in a Thermo Scientific Lab-line vacuum oven (Waltham, MA) at room temperature and −13 psi. ATR-FTIR and elemental analysis were also conducted on the dried samples (see above for details). In these experiments the goal was to prepare samples where the PL and NMR of photobleached CACDs could be directly compared, rather than measuring the photobleaching kinetics which were determined in separate experiments described below.

Photobleaching kinetics: Borosilicate glass tubes (16 mm O.D. x 125 mm) sealed with PTFE-lined caps were filled with 8 mL of a 15 mg/L solution of CACDs. Tubes were placed into a rotating carousel in a Rayonet photoreactor and irradiated with 350 nm light using either 16 or 4 bulbs. Irradiation times when using 16 bulbs were 0, 2, 5, 10, 20, 30, 60, 120, 180 and 720 min. When 4 bulbs were used irradiation times were 0, 8, 20, 40, 80, 120, 240, 480, and 720 min. At each time point, two replicates were removed and replaced with non-irradiated tubes of CACDs. PL measurements on each sample were conducted as described above.

Cysteine: Borosilicate glass tubes (16 mm O.D. x 125 mm) sealed with PTFE-lined caps were filled with 8 mL of 15 mg/L CACDs with L-cysteine added at concentrations of 0, 2, 5, 10, 25, or 50 mM. CACD-cysteine solutions were placed into a rotating carousel in a Rayonet photoreactor and irradiated with 350 nm light for 20 min. PL was conducted on each sample, without further dilution, as described above.

Citrazinic acid experiments: Borosilicate glass tubes (16 mm O.D. x 125 mm) sealed with PTFE-lined caps were filled with 8 mL of 15 mg/L citrazinic acid (CZA), prepared by sonicating CZA in HPLC-grade water for 30 min or until complete dissolution. CZA solutions were placed into a rotating carousel in a Rayonet photoreactor and irradiated with 350 nm light for 0, 3, 8, 12, 20, and 30 min. The photodegradation of citrazinic acid and formation of any photoproducts over time was determined using liquid chromatography coupled with high resolution mass spectrometry. For this, a Thermo Scientific UltiMate 3000 RSLCnano UHPLC (binary bump, degasser, autosampler, and column oven) was coupled to a Q-Exactive HF Orbitrap (Thermo Scientific). All samples were analyzed in positive/negative electrospray ionization mode. A Hydro-RP C18 (Phenomenex) column was used for chromatographic separation with an injection volume of 10 μL. A gradient mobile phase method with 0.1 % formic acid in Milli-Q Water (A) and methanol (B) as eluents was employed to facilitate separation of CZA and any phototransformation products. The initial conditions of the eluents were 95 % (A) and 5 % (B) from 0 to 2 min, followed by linear change of (B) to 95 %

from 2 to 8 min, continued 95 % (B) from 8 to 14 min, and ended with a return to 5 % (B) from 14 to 20 min. The flow rate was set to 75 μL min^{-1}. Data-dependent acquisition was used to collect MS^2 spectra as described: a full scan (100–300 *m/z*) was obtained and followed by MS^2 collection for the seven most abundant ions.

3. Results and discussion

Initial CACD characterization. Citric acid and ethylenediamine CDs (CACDs) were chosen because they are a well-characterized and commonly produced type of CD due to their high quantum yields and ease of synthesis [9,93,94]. The optical properties of CACDs are characterized by strong excitation-independent blue-green fluorescence centered at 470 nm and absorbance that occurs below 400 nm, with a characteristic peak at approximately 350 nm attributed to the n-π^* transition of C–N or C=O bonds, and a shoulder at approximately 230 nm attributed to π-π^* transition of aromatic C=C bonds (Fig. S1(A)) [27,95].

The CACD fluorescence appears as the convolution of two PL peaks contributing to the overall emission spectrum. This is shown in PL spectra recorded prior to the onset of photobleaching; the t = 0 min trace in Fig. 1 and also in Figs. S3 and S8. Upon irradiation with 350 nm light, CACDs rapidly undergo photobleaching. As shown in Fig. 1, over 50 % of the CACD fluorescence is lost after 10 min of continuous irradiation and completely disappears after 12 h. The observation of photobleaching in CACDs is consistent with other CDs synthesized via bottom-up methods, in which fluorescence is attributed to molecular fluorophores [46,47].

Although analytical techniques such as X-ray photoelectron spectroscopy (XPS) and ATR-FTIR are frequently used to characterize the chemical functional groups present in CDs [52,93,96,97], these methods lack the molecular specificity or sensitivity to capture the detailed chemical environments associated with the CD fluorophore. These issues were exemplified in our previous work on photobleaching CDs synthesized with ethylenediamine and citric or malic acid [68], where we did not detect any significant changes in CDs using ATR-FTIR or XPS after irradiation with sunlight, despite the observation that CDs underwent an obvious and permanent loss of fluorescence. For CDs synthesized with citric acid and urea, others have reported observing changes in ATR-FTIR spectra following irradiation with UV light, including the loss or growth of relatively sharp peaks associated with N–H, C–H, and C=O bonds [69,70].

Here, ATR-FTIR and elemental analysis were conducted on CACDs before and after irradiation with 350 nm light. The ATR-FTIR spectrum of as-synthesized CACDs (Fig. S1(B)) exhibits absorption features at approximately 3200 cm^{-1}, corresponding to O–H and N–H stretching modes [68,82,93,95], approximately 1700 cm^{-1} and 1650 cm^{-1}, which are indicative of stretching modes in carboxyl and amide moieties, respectively, and at approximately 1550 cm^{-1}, corresponding to N–H bending in amide groups [68,93,95]. ATR-FTIR of CACDs following irradiation with 350 nm light is shown in Fig. S2, demonstrating that no major changes in chemical bonding occur when CACDs are photobleached, except for a slight decrease in the intensity of the peak at 1550 cm^{-1} for the longer irradiation times. CACD elemental composition before and after irradiation is reported in Table S1, and again, no major changes are seen as a result of photobleaching. The average elemental composition of CACDs is 44.51 % C, 5.05 % H, and 13.26 % N. The average C content of CACDs after 4 h of irradiation is only slightly lower than before irradiation, with 44.73 % and 42.66 %, respectively.

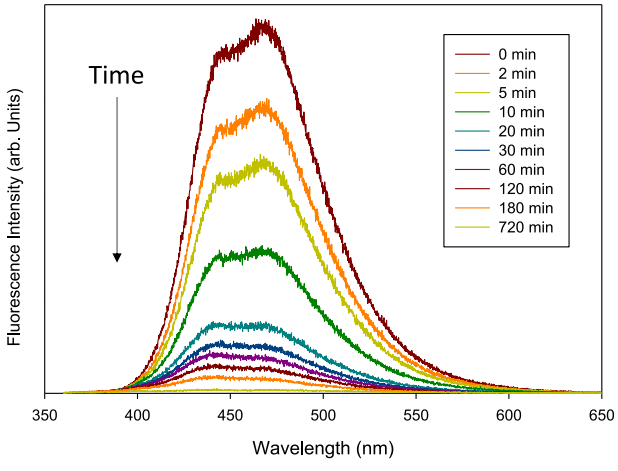

Fig. 1. Photobleaching of CACDs irradiated with 350 nm light measured by the change in PL.

Application of solution-phase NMR. In principle, solution-phase NMR can provide the molecular specificity needed to probe the structure of CDs, opening up opportunities for quantitative and structural analyses. Indeed, although there are reports of ^{1}H NMR on CDs in the literature [52], the spectra are of limited value due to the narrow distribution of chemical shifts associated with different proton bonding environments. This leads to complex ^{1}H NMR spectra where the contributions from specific functional groups and components within the CD (e.g., the fluorophore) are difficult to discern and quantify. In contrast, the carbon nucleus being in proximity to multiple electron pairs leads to a broader chemical shift range in ^{13}C NMR, and the rarity of $J_{C\text{-}C}$ coupling due to naturally low ^{13}C abundance, combined with the ease with which proton-carbon ($J_{C\text{-}H}$) decoupling can be achieved on modern spectrometers, makes ^{13}C NMR a powerful analytical tool for interrogating the structure and properties of CDs [98]. However, ^{13}C NMR spectra of CDs are rarely reported in the literature and typically feature poor signal-to-noise ratios or excessive data processing (e.g., exponential line broadening) that preclude quantitative analysis. The reason for this is partly a consequence of the fact that the natural abundance of the NMR-active ^{13}C isotope is low (1.1 %), so without high field spectrometers and excessively long analysis times, it is difficult to acquire ^{13}C spectra with an acceptable signal-to-noise ratio for quantitative purposes.

The other issue with acquiring quantitative ^{13}C NMR on CDs relates to the relatively low sensitivity of NMR [97,99]. It is important to note that CD concentrations used in NMR analyses are typically not reported in the literature [9,18,60,61,78,80,82–85]. However, reported CD concentrations are on the order of 4–17 mg/mL [68,74,81], or 2–10 mg of CDs, concentrations that generate qualitative ^{13}C spectra on a 400 MHz spectrometer. Similarly, in our initial attempts to conduct ^{13}C NMR on CACDs, we started with approximately 10 mg per sample and many of the peaks in ^{13}C spectrum were barely discernible above the baseline (Fig. 2(C)). However, CDs possess a negative surface charge (−10.6 mV for the CACDs used in this study) [100], are extremely small (<10 nm), and are comprised of relatively low Z elements (C, N, O, H). Collectively, these attributes impart extreme water solubility to CDs [81]. As a consequence, we realized that we could increase the concentration of CDs considerably above previously used values, reaching a solubility limit of 400 mg CACDs in 600 μL D_2O. Fig. 2 shows ^{1}H and ^{13}C NMR spectra of samples containing 10 mg of CACDs (Fig. 2(A) and (C), top) versus 400 mg of CACDs (Fig. 2(B) and (D), bottom) in 600 μL D_2O. Results presented in Fig. 2 show that although the ^{1}H spectra for both concentrations are comparable in terms of signal to noise, these much higher CD concentrations open up the possibility of using ^{13}C NMR for quantitative analysis. Compared to most nanoparticles, the small (<10 nm diameter) size of CACDs also facilitates peak assignments and integration which can be challenging for ligands associated with larger nanoparticles due to slow particle rotation speeds and corresponding line broadening [99]. However, it is important to note that although CDs are small nanoparticles they are still relatively large compared to molecular NMR analytes and thus, it is necessary to allow for a sufficiently

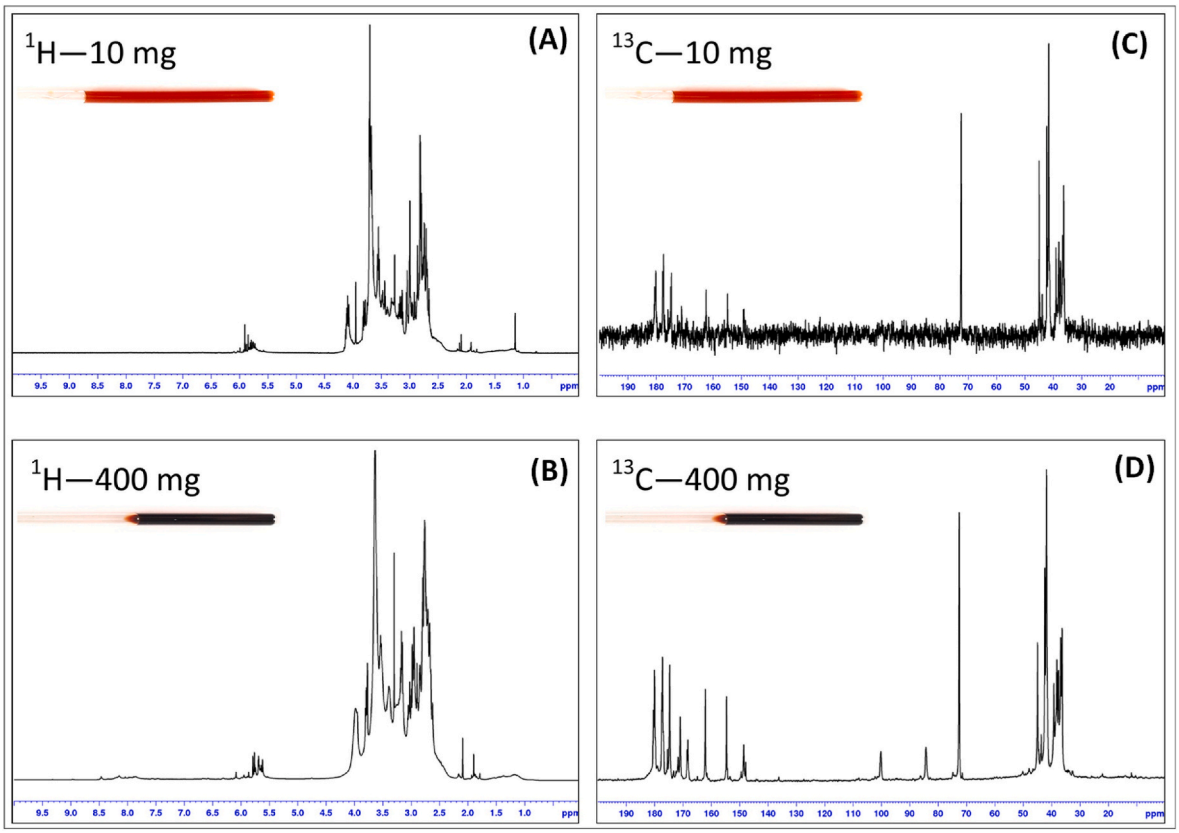

Fig. 2. NMR spectra of CACDs at different concentrations. Top row: 10 mg CACDs in 600 μL D_2O, A) ^{1}H NMR and C) ^{13}C NMR. Bottom row: 400 mg CACDs in 600 μL D_2O, B) ^{1}H NMR, D) and ^{13}C NMR. Photographs of NMR tubes containing CACD samples used for analysis are inset.

long T_1 relaxation delay when collecting ^{13}C NMR spectra. Experimentally, we determined that the T_1 relaxation time for CACDs was 1.77 s or less, and for all subsequent NMR analyses we used a relaxation delay of 10 s to ensure that all ^{13}C data was quantitative.

NMR of CDs. As discussed above, the ^{1}H spectrum (Fig. 2) is complicated by the overlapping signals especially in the range of 2.5–4.0 ppm, which corresponds to protons either bound to or in the α-position to a number of oxygen-containing functional groups, including alcohol, ether, and ester moieties [68,81]. Additionally, clusters of proton signals appear in the ranges of 1.8–2.5 and 5.5–6.3 ppm, indicating the presence of allylic protons or protons in an α- or β-position relative to carbonyl or amide groups and vinylic protons (H bound to C in C=C), respectively. Signals from 7.8 to 8.5 ppm correlate to non-exchangeable amide protons or protons bound to aromatic rings [68,81], and these signals are notably absent from the lower concentration (10 mg) ^{1}H spectrum. There is also a broad signal from 1.0 to 1.5 ppm which corresponds to protons in alkyl groups, which is sharper in the lower concentration ^{1}H spectrum.

Fig. 2 shows the corresponding ^{13}C spectra of the same CACD samples. The major groups of signals in the ^{13}C spectrum can be classified as follows: signals from 0 to 30 ppm correspond to alkanes, from 30 to 60 ppm correspond to C–N in amine groups, from 65 to 75 ppm correspond to C–O in alcohols and ethers, from 80 to 160 ppm are representative of sp^2 carbons in alkenes and aromatic rings, and from 160 to 185 ppm are carbon atoms in amides and carbonyls, including ester and carboxyl groups [27,68]. Several of these signals are absent or indiscernible above the baseline in the 10 mg CACD ^{13}C spectrum in Fig. 2(C), especially those corresponding to sp^2 carbons. In the 400 mg sample (Fig. 2 (D)), the peaks associated with sp^2 carbons and C–O are sharp and individually resolvable, in contrast to the clusters of peaks from approximately 30-50 and 165–180 ppm.

The solution phase ^{13}C NMR spectra shown in Fig. 2(D) is also consistent with the quantitative solid state ^{13}C NMR of CACDs (synthesized using the same precursors) shown in ref. [96], the later exhibiting peaks centered at ≈ 40, 180 and 70 ppm as well as additional discrete peaks between 80 and 160 ppm, each of similar relative intensities to those shown in Fig. 2(D). The broad qualitative and quantitative similarities between the solution and solid state ^{13}C NMR of CACD provides strong support for the idea that the sonication required to disperse the CACD in the present study for NMR did not produce any degradation or transformation of the CACD. This assertion is also supported by the invariant nature of the ATR-IR we observed for CACD before and after sonication.

NMR of Photobleached CACDs. ^{13}C NMR spectra of photobleached CACDs with progressively less fluorescence (from top to bottom) are shown in Fig. 3; the corresponding PL data is shown in Fig. S3. A number of changes in the spectra occur during photobleaching, including small and subtle changes to the clusters of peaks representing amine (30–60 ppm), amide and carbonyl species (160–185 ppm). However, the most obvious change in the ^{13}C NMR spectra is the systematic decrease in intensity of the six peaks between 80 and 170 ppm that occurs as the fluorescence intensity of the CACDs decreases. Fig. 4 highlights this region of the ^{13}C NMR spectrum between 75 and 175 ppm, showing the six peaks of interest located at approximately 85, 100, 148, 155, 162, and 168 ppm. These six peaks have previously been identified as corresponding to carbon atoms in IPCA, shown in Fig. 4 along with the ^{13}C peak assignments. The remaining two C atoms cannot be clearly resolved because they overlap with peaks associated with the CACD polymeric core. IPCA has been previously identified as a molecular fluorophore in citric acid and ethylenediamine CDs [59,96]. The peak assignments were further confirmed with 2D heteronuclear single quantum coherence (HSQC) and heteronuclear multiple bond correlation (HMBC) spectra, shown in Figs. S4 and S5, respectively, which also agree with previously reported IPCA spectra [59]. In addition to ^{13}C

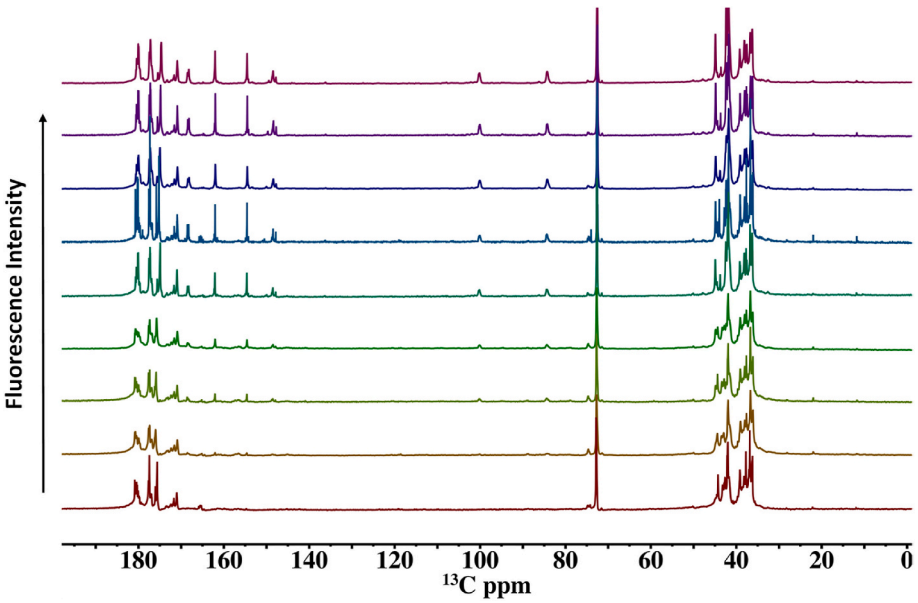

Fig. 3. ^{13}C NMR spectra of CACDs photobleached at 350 nm. The uppermost spectrum represents as-synthesized CACDs and each subsequent spectrum shows CACDs with decreasing fluorescence due to photobleaching.

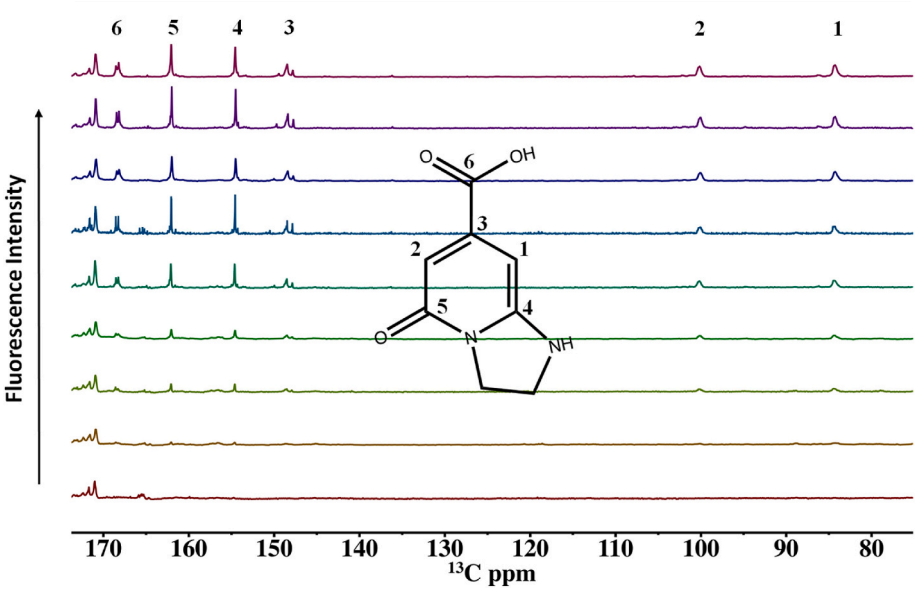

Fig. 4. Expanded view of the 75–175 ppm region of the CACD ^{13}C spectra from Fig. 3 with the IPCA molecule overlaid. The six IPCA peaks that decrease in intensity as the CACD fluorescence decrease are labeled and assigned to six carbons in the IPCA molecule.

NMR, Fig. 5 shows the ^{1}H NMR spectra for all photobleached CACDs. Some subtle changes are observed in the broad range of peaks between 2.5 and 4.0 ppm although the most obvious change is the loss in intensity that occurs for the aromatic protons located at approximately 5.8 ppm, corresponding to aromatic protons associated with the IPCA chromophore, identified as such by 2D HSQC and HMBC. Notably, the decrease in intensity associated with these aromatic protons occurs at the same rate as the decrease in intensity observed for the IPCA ^{13}C NMR peaks (compare Figs. 4 and 5).

State of the IPCA Chromophore: In principle the IPCA chromophores detected by NMR could be part of the carbon dot or be present as isolated molecules in solution. To answer this question, we conducted Diffusion ordered spectroscopy (DOSY) on CACD in D_2O. DOSY is an NMR method wherein signals of different species in a complex mixture are separated according to their diffusion coefficient. An isolated molecule in solution (e.g. water with a ^{1}H peak position of 4.7 ppm) diffuses more quickly relative to a much larger species (e.g. 2–5 nm diameter CACD) [27,95]. Thus, any unbound or weakly associated IPCA molecules would have a diffusion coefficient significantly faster than CACD. The DOSY spectrum of CACDs (Fig. 6) reveals that ^{1}H NMR peak associated with IPCA at ~5.6 ppm and the ^{1}H protons associated with the polymeric fraction of the CACD located between 1.5 and 4.2 ppm have the same diffusion coefficient. In contrast, the diffusion coefficient of the ^{1}H NMR protons associated with water is more than one order of magnitude higher. Thus, Fig. 6 reveals that all of the IPCA molecules are trapped within or covalently bound to the CACD, but are not present as isolated molecules freely rotating in solution.

Correlation of NMR spectra with PL for photobleached CDs. As described in the experimental section, PL and NMR data were acquired from the same powdered CD samples that were photobleached. This was done

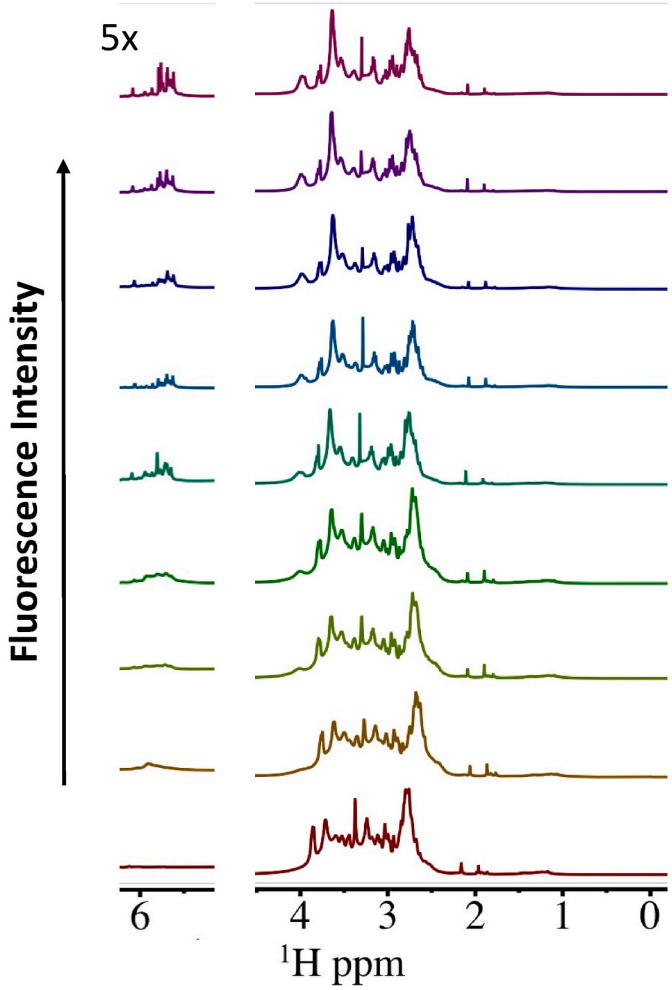

Fig. 5. ^{1}H NMR spectra of CACDs photobleached at 350 nm. The uppermost spectrum represents as-synthesized CACDs and each subsequent spectrum shows CACDs with decreasing fluorescence as a consequence of photobleaching.

deliberately to ensure that the fluorescence intensity of the photobleached CDs shown in Fig. S3 could be directly compared to the corresponding ^{13}C NMR shown in Fig. 3. To quantify the fractional decrease in the concentration of IPCA molecules in photobleached CDs it was necessary not only to ensure the ^{13}C NMR itself was obtained quantitatively by using a sufficiently long relaxation time but also to have an internal reference within the ^{13}C NMR itself so that any sample-to-sample signal variations could be compensated. This internal calibration was achieved by taking the ratio of the IPCA peaks to the intense C–O peak observed between 65 and 75 ppm (see Fig. 3) which remained invariant during the photobleaching process. The invariant nature of the C–O peak was itself verified by comparing ^{13}C NMR spectra of CDs at various stages of photobleaching to a TMSP standard (Fig. S6).

Using this approach, the total integrated area of the six IPCA peaks shown in Fig. 4 was measured and referenced to the C–O peak area acquired in the same ^{13}C NMR spectra. This information was then used to determine the relative IPCA concentration in each photobleached CD referenced to the IPCA concentration in the CD prior to photobleaching. The obtained value was plotted against the corresponding fluorescence intensity of the CD as determined by the PL area (from Fig. S3). The results of this analysis, shown in Fig. 7(A) reveal that there is a strong linear correlation (R^2 = 0.9856) between the PL intensity and the fractional concentration of IPCA in the CDs. Fig. 7(B) shows the same data but plotted for each individual IPCA NMR peak shown in Fig. 4,

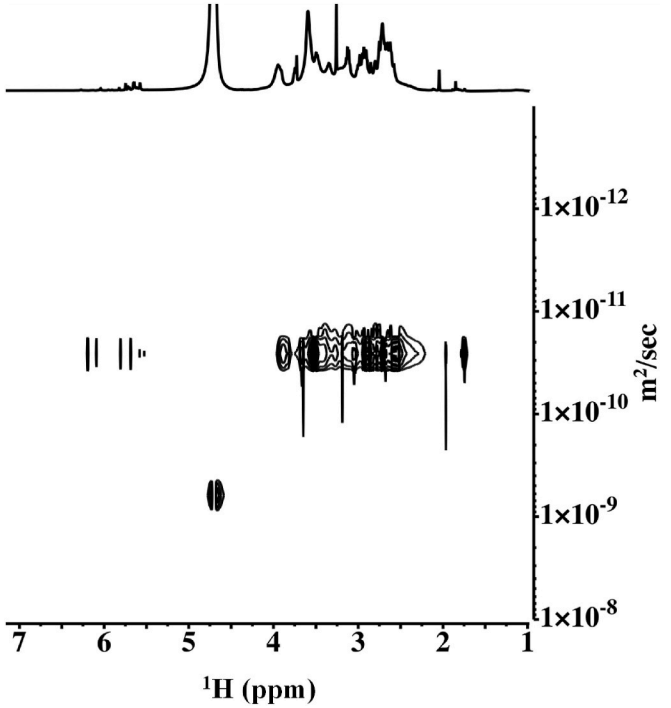

Fig. 6. ^{1}H DOSY spectrum of CACDs in D_2O.

revealing that each of the six peaks decrease at the same rate as the CDs are photobleached, consistent with the idea that each of these six peaks are associated with the IPCA fluorophore. The linear dependence of the CACD fluorescence on the IPCA concentration indicates that the IPCA molecules are behaving as isolated chromophores within the CD.

Of significance, Fig. 7 demonstrates that although there is a linear correlation between the relative IPCA concentration and the fluorescence intensity of the CACD, this correlation curve does not pass through the origin. Specifically, when there is no detectable IPCA concentration left in the CACD (i.e., the *y*-intercept in Fig. 7), the fluorescence intensity has decreased by only 84 % of its initial value. In the context of the ^{13}C NMR data this is evidenced by the observation that although the most photobleached CACD shown in Fig. 4 (the lowermost orange trace) contains no detectable IPCA the CACD remains fluorescent as shown in Fig. S3 (the lowermost orange trace). Consequently, IPCA alone is not responsible for all of the CACD fluorescence. In other words, another fluorophore must be present. Specifically, our results indicate that while the IPCA molecules are responsible for the overwhelming majority of the fluorescence of the CACDs, 16 % of the nascent CACD fluorescence emanates from a second type of fluorophore. Moreover, since this residual fluorescence persists when all of the IPCA molecules have been photobleached, the other fluorophore must be significantly more photostable than IPCA. Qualitatively, this is also consistent with the photobleaching kinetics shown in Fig. 8(A) and S8, which reveal a rapid loss of approximately 80 % of the fluorescence intensity during the initial 30 min of irradiation followed by slower photobleaching of the remaining 16 % over the course of several hours.

Evolution of the fluorescence spectrum. Based on the NMR analysis, the fluorescence spectra observed when the CDs have lost more than 84 % of their nascent intensity must be due solely to the minor fluorophore because all of the IPCA has been photodegraded. Conversely, prior to photobleaching, 84 % of the fluorescence intensity is determined by IPCA. These two pieces of information enable us to deconvolute the fluorescence spectrum of the nascent CDs into the contribution from IPCA molecules and the other less intense fluorophore. Results of this analysis are shown in Fig. 8(B). The NMR analysis also demonstrates that IPCA photobleaching reaches completion before any measurable

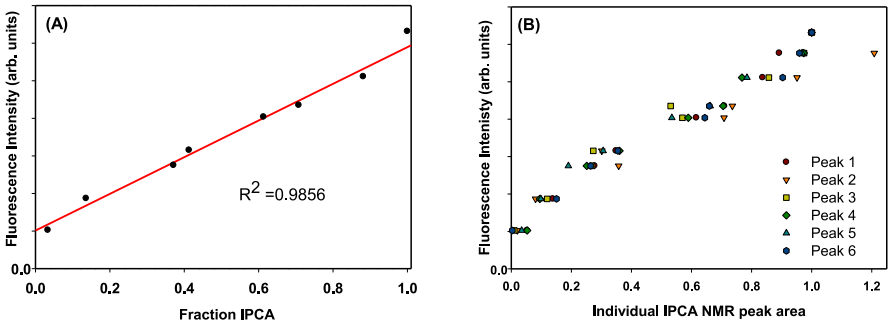

Fig. 7. Correlation plot between CACD fluorescence as measured by PL (see Fig. S3) during the photobleaching process and the normalized concentration of IPCA within the CACD as determined by ^{13}C NMR based on (A) the total integrated area of all six of the IPCA peaks and (B) each individual IPCA peak, as shown in Fig. 4.

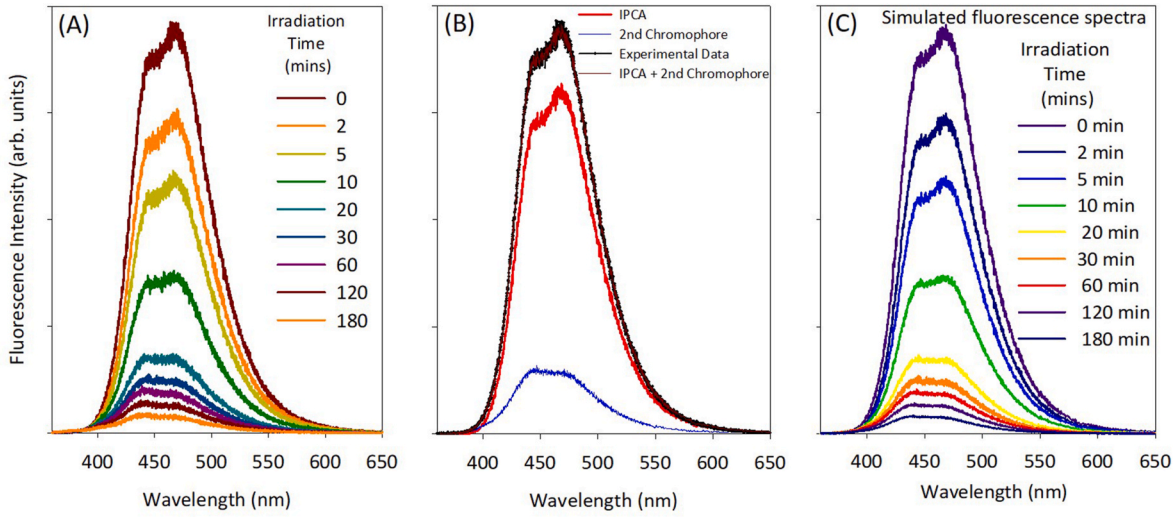

Fig. 8. Evolution of the fluorescence spectra during photobleaching. (A) Experimental data; (B) deconvolution of the initial (t = 0 min) CACD fluorescence spectra into the contributions from the two fluorophores based on ^{13}C NMR analysis (see text for details); (C) simulated evolution in the fluorescence spectra, predicted on the basis of the fluorescence line shapes associated with the two fluorophores shown in (B) and their photostabilities (see text for details).

photodegradation of the other, less intense, fluorophore occurs. Since Fig. 8(B) provides us with the fluorescence spectra associated with these two fluorophores we can use this information on their relative photostability to simulate how the fluorescent spectrum is predicted to evolve as the CD is photobleached. The results of this analysis, shown in Fig. 8 (C) reveal that this simulation provides an extremely good fit to the experimentally observed evolution of the fluorescence spectra. This provides strong support for the idea that the fluorescence spectra are composed of contributions from two distinct fluorophores with slightly different emission characteristics and significantly different photostability.

This qualitative kinetic analysis can also be compared with the evolution in the fluorescence spectrum as a function of increasing irradiation time (Fig. 8(A)) which shows that during the initial stages of photobleaching (<30 min), when approximately 80 % of the fluorescence intensity is lost, the spectral envelope changes with the peak at approximately 470 nm decreasing more rapidly than the shoulder centered around 440 nm. In contrast, for more prolonged irradiation times (>30 min), when the overall fluorescence intensity has decreased to < 20 % of its initial value, the line shape of the fluorescence spectrum remains constant as the intensity decreases with increasing irradiation time. The relative change in the intensity of the fluorescence peaks at 470 nm (I(470)) and 440 nm (I(440)) during irradiation is shown quantitatively in Fig. S7, where the I(470)/I(440) ratio has been plotted as a function of irradiation time. Fig. S7 shows that there is a decrease in I(470)/I(440) over the 30mins irradiation timescale over which the NMR data shows that the IPCA is photobleached and afterwards the I (470)/I(440) ratio remains virtually constant because the remaining spectral envelope is now associated with a single fluorophore that is being more slowly photodegraded. These analysis of the evolution of the fluorescence spectrum during photobleaching is therefore also consistent with the NMR data because it implies the presence of two fluorophores, specifically a more intense but more photolabile component (IPCA) along with a second less intense, but more photostable component.

Photobleaching kinetics. Figs. S8 and S9 show the results of kinetic experiments comparing the photobleaching rates of CACDs irradiated with sixteen 350 nm bulbs (Fig. 1) versus with CACDs irradiated with four 350 nm bulbs over longer irradiation times. When normalized by the relative photon flux, the PL decay curves in Fig. S9 are virtually identical, demonstrating that for each fluorophore the rate determining step in photobleaching is a one-photon process. This agrees with previous laser-induced photobleaching studies where the photobleaching rate of carbon dots synthesized from urea and citric acid was seen to follow the same dependence on energy input across a range of laser powers, indicative of a single photon absorption event that leads to irreversible photobleaching [47].

The relative photostabilities of the two fluorophores can be determined from the photobleaching kinetic data shown in Fig. 9. Based on the NMR analysis we can model the loss of fluorescence intensity as arising from a linear contribution from two fluorophores with different photostabilities, using the following equation:

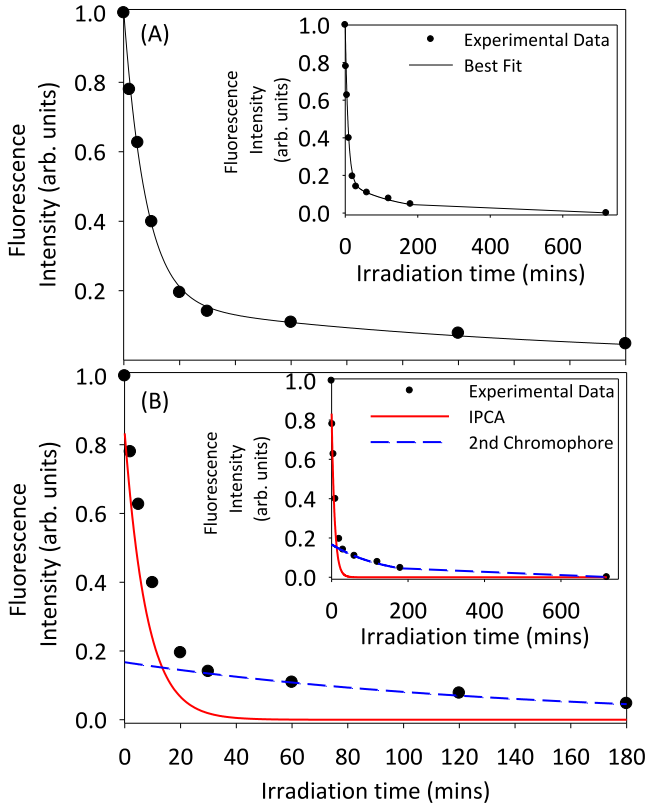

Fig. 9. Photobleaching kinetics. (A) Experimental data (solid circles) along with the best fit solid line based on the photobleaching of the two fluorophores determined from Equation (2) – see text for details; (B) relative contribution to the fluorescence from the two fluorophores as a function of irradiation time: IPCA contribution is shown by the red line and the second fluorophore by a blue dotted line. Inserts in (A) and (B) show the photobleaching kinetics and the relevant fits with a prolonged irradiation (780 min) time point added. (For interpretation of the references to colour in this figure legend, the reader is referred to the Web version of this article.)

$$\frac{I_t}{I_{t=0}} = 0.84\, e^{-k_{IPCA}t} + 0.16\, e^{-k_A t} \tag{2}$$

Where I_t represents the CACD fluorescence intensity at time t, k_{IPCA} represents the photobleaching rate constant for IPCA and k_A represents the photobleaching rate constant for the second, less intense fluorophore. The 0.84 and 0.16 values represent the fractional contributions to the fluorescence intensity from the two fluorophores in the as-synthesized CACDs prior to photobleaching (i.e., $t = 0$) based on the NMR analysis. The best-fit results of this analysis are shown as the solid line in Fig. 9(A), while in Fig. 9(B) the fractional contributions from the two fluorophores to the total fluorescence during the photobleaching process are shown. Analysis of Fig. 9(A) reveals that this two-species model provides an excellent fit to the overall photobleaching kinetics ($R^2 = 0.998$) and reveals that IPCA is 18 times more photolabile than the other fluorophore, consistent with the inference of the NMR analysis in Fig. 7 that over the course of the irradiation time necessary to photobleach all of the IPCA the other fluorophore is photochemically stable as shown in Fig. 9(B). It is worth noting that an analogous multi-component exponential fitting has been found necessary to accurately describe the photobleaching kinetics for a heterogeneous set of CDs synthesized from different precursors using different methods and exhibiting different fluorescent properties [70].

The success of Equation (2) in modeling the photobleaching kinetics implies that for CDs synthesized from citric acid and ethylenediamine the two fluorophores (including IPCA) have photostabilities independent of their local environment. However, the heterogeneity of the local environment encountered by fluorophores within CDs (e.g., conformations within CDs or monomeric vs dimer stacked IPCA) provides a rationale for the more structured emission profile we observe for IPCA fluorophores incorporated within CACDs (see Fig. 8(B)), as compared to isolated IPCA molecules in solution. This is also consistent with previous time-resolved PL data which could only be well fit using a stretched exponential fit, suggesting that that the molecular fluorophores responsible for CD fluorescence experience a degree of heterogeneity in their local environments [47]. Indeed, the existence of heterogeneous local environments for the IPCA molecules within CACDs is evident from the NMR data shown in Fig. 4. Notably, although the integrated intensities of the six discernible IPCA peaks (Fig. 7) are similar to one another, as expected based on the IPCA structure, the peak shapes differ significantly; for example, the C6 and C3 peaks in IPCA exhibit measurable splitting, whereas the ^{13}C NMR of isolated IPCA molecules should produce only a single peak.

Second fluorophore. Both the NMR/PL and kinetics experiments independently support the idea of two fluorophores contributing to CACD fluorescence, with IPCA as the primary component, along with an undetermined more photostable, secondary component. We posit that the secondary component is associated with nitrogen-containing polycyclic aromatic hydrocarbons embedded within or as part of the conjugated carbon/aromatic core, which others have proposed as a source of CD fluorescence [43,59,101–104]. Indeed, in our companion study where we have used solution phase ^{1}H and ^{13}C NMR to probe the structure of CACD [105], we have found experimental evidence for the existence of large-scale delocalized graphenic sheets associated with an aromatic core. This evidence comes by means of saturation transfer experiments involving ^{1}H NMR, where even a weak saturation pulse applied briefly anywhere in the aromatic region devoid of visible signal (6.5–7.5 ppm) in the ^{1}H NMR (see Fig. 5) causes, the polymeric signals to be significantly attenuated. This suggests the presence of an aromatic component within CACDs that is not visible directly by routine 1D ^{1}H or ^{13}C NMR. An analogous approach has recently been used to uncover NMR-invisible fractions in a wide range of different polymers [106]. We believe that the NMR signatures for the second fluorophore are contained within this aromatic core.

The idea that the conjugated carbon/aromatic core can contribute to the overall fluorescence of CD is in accord with several other studies, in which the primary source of CD fluorescence evolves with increased reaction temperatures and reaction times during CD synthesis, from molecular fluorophore to CD core. These changes in synthesis conditions lead to CDs with lower QYs but greater photostability, aligning with our observations [32,59,104,107]. Indeed, a protective effect of the carbon core against photobleaching has been proposed in previous studies [50], while Wang et al. [32] have proposed that fluorophores within the core would have lower QYs due to energy dissipation throughout the conjugated carbon/aromatic core. Another important corollary of this argument is that for CACDs synthesized with other methods (e.g., hydrothermal, higher/lower temperatures), the relative contribution of IPCA and the carbon core to the CACD fluorescence may well differ from those values determined in the present study.

Fig. S10 shows that by adding cysteine to the solution the rate of photobleaching decreased systematically as the cysteine concentration increased. Since cysteine is a known singlet oxygen quencher [88], these results indicate that singlet oxygen is a ROS involved in the photobleaching process. Related work has previously shown that photobleaching can also be inhibited by the introduction of radical scavengers (e.g., ascorbic acid), or by depriving CD solutions of oxygen, demonstrating that CD photobleaching is mediated by ROS formed in the presence of dissolved oxygen in solution [68,69,108,109]. With respect to the two types of fluorophores identified in this study, the less intense fluorophore embedded within the CD core might reasonably be expected to be more photostable than the molecular IPCA fluorophores distributed closer to the surface of the CDs, consistent with our experimental

observations.

Phototransformation products of IPCA. To investigate the type of photoproducts that could be generated during the photobleaching of nitrogen containing heterocycles such as IPCA we used high-resolution mass spectrometry to identify transformation products generated when citrazinic acid (CZA) is exposed to 350 nm irradiation. CZA [50,110–113] is an inexpensive commercially available nitrogen containing heterocycle that has been used as a model compound for both experimental and computational explorations into the behavior of CD molecular fluorophores [47,64,110–114]. CZA is particularly useful as a model fluorophore for CACDs because CZA absorbs and emits light at similar wavelengths to citric-acid based CDs, 365 nm and 440 nm, respectively [114]. In this study, CZA was used as a model fluorophore to determine the type of chemical transformations IPCA may undergo during photobleaching. The results identified one phototransformation product. The MS/MS spectrum of CZA (Fig. S11(A)) shows the parent mass ion at m/z 154 along with two fragment peaks. Fig. S11(B) shows the mass spectrum and proposed chemical structure of the phototransformation product (labeled TP-170) with a parent ion mass at m/z 170 as well as main fragment peaks associated with CO_2 loss followed by two CO loss peaks. These findings indicate that the carboxylic acid group present in CZA remains intact in the phototransformation product, which also contains two carbonyl groups. These structural characteristics are consistent with the proposed TP-170 structure which can be identified as a phototransformation product because its peak area increases as the CZA peak area decreases as a function of 350 nm irradiation time (see Fig. S11(C)). It should be noted that TP-170 is also detected in the starting material, possibly as a result of unintended exposure to light during CZA synthesis and/or storage. Based on the structure of CZA and TP-170, we can propose a transformation mechanism shown in Fig. S11(D) that is initiated by the electrophilic 4 + 2 addition of $^1O_2$ across the delocalized π-system in CZA, similar to cycloaddition reactions of $^1O_2$ with other nitrogen containing heterocycles including 2-pyridone derivatives such as IPCA [115,116], followed by the elimination of H_2O to form TP-170. It is therefore likely that analogous photoproducts would be formed in the reaction of $^1O_2$ with IPCA. The predicted ^{13}C NMR of such species indicates that their appearance would contribute to the subtle changes we observed in the regions between 50-30 ppm and 160–190 ppm.

4. Conclusions

In this work, we demonstrate the application of quantitative solution phase ^{13}C NMR as a way to observe chemical transformations occurring as a consequence of photobleaching within CDs synthesized from citric acid and ethylenediamine. We have shown that high concentrations of CACDs (667 mg/mL) can remain colloidally stable, opening up the opportunity to acquire quantitative ^{13}C NMR spectra. Monitoring changes in ^{13}C NMR during photobleaching has revealed that there is a linear correlation between the CD fluorescence and the concentration of IPCA and that this fluorophore is responsible for the vast majority (>80 %) of CACD fluorescence, with the residual contribution arising from a more photostable fluorophore, which exhibits similar fluorescence properties to the IPCA. The existence of these two sources of fluorescence allows us to accurately describe the evolution of the fluorescence spectrum during photobleaching as well as the photobleaching kinetics of CACDs.

It is important to note that, in principle, quantitative solution phase ^{13}C NMR data could also be acquired for CDs other than the CACDs that were the focus of this study, because the combination of small size, negative surface charge, and low van der Waals forces of attraction are common to almost all bottom-up synthesized CDs. If a sufficient quantity of CDs is synthesized, the experimental approach described in this study, comparing changes in fluorescence during photobleaching to corresponding changes in the ^{13}C NMR spectrum, could then be employed as a means to identify the ^{13}C NMR peaks associated with molecular chromophores in other bottom-up synthesized CDs. This would include not only CDs synthesized from other small molecular precursors, but also CDs derived from the larger molecular building blocks used to create CDs from biomass, for example. The ^{13}C NMR data obtained would provide a molecular fingerprint of the fluorophore(s), providing a direct spectroscopic method to identify their chemical composition and structure based on a comparison between experimental data and theoretical predictions. Similarly, quantitative ^{13}C NMR could also be employed to study molecular-level processes associated with other important CD properties, such as the mechanism of metal ion sensing.

CRediT authorship contribution statement

Leslie R. Sigmon: Writing – review & editing, Writing – original draft, Software, Methodology, Investigation, Formal analysis, Data curation, Conceptualization. **Jonathan Catazaro:** Methodology, Investigation, Data curation, Conceptualization. **Mohammed Abdel-Rahman:** Software, Investigation. **Casey Smith:** Writing – review & editing, Data curation. **Carsten Prasse:** Writing – review & editing, Formal analysis, Data curation. **D. Howard Fairbrother:** Writing – review & editing, Writing – original draft, Supervision, Methodology, Investigation, Funding acquisition, Formal analysis, Data curation, Conceptualization.

Declaration of competing interest

The authors declare that they have no known competing financial interests or personal relationships that could have appeared to influence the work reported in this paper.

Acknowledgements

This work was supported by the National Science Foundation under Grant No. CHE-2001611, the NSF Center for Sustainable Nanotechnology (CSN). LRS also acknowledges support from the NSF-GRFP under Grant No. DGE-1746891. The authors would also like to gratefully acknowledge Professor Cathy Murphy and Dr. Meng Wu (University of Illinois) for initial data that demonstrated the potential to use ^{13}C NMR to follow CACD photobleaching as well as Savannah Phillips (Johns Hopkins University) for the CACD Quantum Yield and Zeta Potential measurements.

Appendix A. Supplementary data

Supplementary data to this article can be found online at https://doi.org/10.1016/j.carbon.2024.119796.

References

[1] G.E. LeCroy, S.T. Yang, F. Yang, Y.M. Liu, K.A.S. Fernando, C.E. Bunker, Y. Hu, P. G. Luo, Y.P. Sun, Functionalized carbon nanoparticles: s'yntheses and applications in optical bioimaging and energy conversion, Coord. Chem. Rev. 320 (2016) 66–81.
[2] J. Liu, R. Li, B. Yang, Carbon dots: a new type of carbon-based nanomaterial with wide applications, ACS Cent. Sci. 6 (12) (2020) 2179–2195.
[3] T. Yuan, T. Meng, P. He, Y.X. Shi, Y.C. Li, X.H. Li, L.Z. Fan, S.H. Yang, Carbon quantum dots: an emerging material for optoelectronic applications, J. Mater. Chem. C 7 (23) (2019) 6820–6835.
[4] S. Khan, N.C. Verma, A. Gupta, C.K. Nandi, Reversible photoswitching of carbon dots, Sci. Rep. 5 (1) (2015) 11423.
[5] G. Leménager, E. De Luca, Y.-P. Sun, P.P. Pompa, Super-resolution fluorescence imaging of biocompatible carbon dots, Nanoscale 6 (15) (2014) 8617–8623.
[6] B. Zhi, Y. Cui, S.Y. Wang, B.P. Frank, D.N. Williams, R.P. Brown, E.S. Melby, R. J. Hamers, Z. Rosenzweig, D.H. Fairbrother, G. Orr, C.L. Haynes, Malic acid carbon dots: from super-resolution live-cell imaging to highly efficient separation, ACS Nano 12 (6) (2018) 5741–5752.
[7] J. Zhang, L. Yang, Y. Yuan, J. Jiang, S.H. Yu, One-pot gram-scale synthesis of nitrogen and sulfur embedded organic dots with distinctive fluorescence behaviors in free and aggregated states, Chem. Mater. 28 (12) (2016) 4367–4374.
[8] F.Y. Yan, D.C. Shi, T.C. Zheng, K.Y. Yun, X.G. Zhou, L. Chen, Carbon dots as nanosensor for sensitive and selective detection of Hg2+ and L-cysteine by means

of fluorescence "Off-On" switching, Sensor. Actuator. B Chem. 224 (2016) 926–935.
[9] S.J. Zhu, Q.N. Meng, L. Wang, J.H. Zhang, Y.B. Song, H. Jin, K. Zhang, H.C. Sun, H.Y. Wang, B. Yang, Highly photoluminescent carbon dots for multicolor patterning, sensors, and bioimaging, Angew. Chem. Int. Ed. 52 (14) (2013) 3953–3957.
[10] H. Nie, M.J. Li, Q.S. Li, S.J. Liang, Y.Y. Tan, L. Sheng, W. Shi, S.X.A. Zhang, Carbon dots with continuously tunable full-color emission and their application in ratiometric pH sensing, Chem. Mater. 26 (10) (2014) 3104–3112.
[11] A. Cayuela, M.L. Soriano, S.R. Kennedy, J.W. Steed, M. Valcarcel, Fluorescent carbon quantum dot hydrogels for direct determination of silver ions, Talanta 151 (2016) 100–105.
[12] Q. Guo, F.L. Yuan, B. Zhang, S.J. Zhou, J. Zhang, Y.M. Bai, L.Z. Fan, T. Hayat, A. Alsaedi, Z.A. Tan, Passivation of the grain boundaries of CH3NH3PbI3 using carbon quantum dots for highly efficient perovskite solar cells with excellent environmental stability, Nanoscale 11 (1) (2019) 115–124.
[13] R.Y. Guo, T. Li, S.E. Shi, Aggregation-induced emission enhancement of carbon quantum dots and applications in light emitting devices, J. Mater. Chem. C 7 (17) (2019) 5148–5154.
[14] H.R. Jia, Z.B. Wang, T. Yuan, F.L. Yuan, X.H. Li, Y.C. Li, Z.A. Tan, L.Z. Fan, S. H. Yang, Electroluminescent warm white light-emitting diodes based on passivation enabled bright red bandgap emission carbon quantum dots, Adv. Sci. 6 (13) (2019).
[15] F. Wang, Y.H. Chen, C.Y. Liu, D.G. Ma, White light-emitting devices based on carbon dots' electroluminescence, Chem. Commun. 47 (12) (2011) 3502–3504.
[16] F.L. Yuan, P. He, Z.F. Xi, X.H. Li, Y.C. Li, H.Z. Zhong, L.Z. Fan, S.H. Yang, Highly efficient and stable white LEDs based on pure red narrow bandwidth emission triangular carbon quantum dots for wide-color gamut backlight displays, Nano Res. 12 (7) (2019) 1669–1674.
[17] Z.F. Wang, F.L. Yuan, X.H. Li, Y.C. Li, H.Z. Zhong, L.Z. Fan, S.H. Yang, 53% efficient red emissive carbon quantum dots for high color rendering and stable warm white-light-emitting diodes, Adv. Mater. 29 (37) (2017).
[18] M. Algarra, L. dos Orfaos, C.S. Alyes, R. Moreno-Tost, M.S. Pino-Gonzalez, J. Jimenez-Jimenez, E. Rodriguez-Castellon, D. Eliche-Quesada, E. Castro, R. Luque, Sustainable production of carbon nanoparticles from olive pit biomass: understanding proton transfer in the excited state on carbon dots, Acs Sustain. Chem. Eng. 7 (12) (2019) 10493–10500.
[19] R. Atchudan, T.N.J.I. Edison, S. Perumal, R. Vinodh, A.K. Sundramoorthy, R. S. Babu, Y.R. Lee, Leftover kiwi fruit peel-derived carbon dots as a highly selective fluorescent sensor for detection of ferric ion, Chemosensors 9 (7) (2021).
[20] R. Atchudan, T.N.J.I. Edison, M. Shanmugam, S. Perumal, T. Somanathan, Y. R. Lee, Sustainable synthesis of carbon quantum dots from banana peel waste using hydrothermal process for in vivo bioimaging, Phys. E Low-dimens. Syst. Nanostruct. 126 (2021).
[21] S. Perumal, R. Atchudan, T.N.J.I. Edison, Y.R. Lee, Sustainable synthesis of multifunctional carbon dots using biomass and their applications: a mini-review, J. Environ. Chem. Eng. 9 (4) (2021).
[22] M.P. Aji, A.L. Wati, A. Priyanto, J. Karunawan, B.W. Nuryadin, E. Wibowo, P. Marwoto, Sulhadi, Polymer carbon dots from plastics waste upcycling, Environ. Nanotechnol. Monit. Manag. 9 (2018) 136–140.
[23] S. Chaudhary, M. Kumari, P. Chauhan, G.R. Chaudhary, Upcycling of plastic waste into fluorescent carbon dots: an environmentally viable transformation to biocompatible C-dots with potential prospective in analytical applications, Waste Manag. 120 (2021) 675–686.
[24] Y. Xiong, J. Schneider, E.V. Ushakova, A.L. Rogach, Influence of molecular fluorophores on the research field of chemically synthesized carbon dots, Nano Today 23 (2018) 124–139.
[25] S. Chahal, N. Yousefi, N. Tufenkji, Green synthesis of high quantum yield carbon dots from phenylalanine and citric acid: role of stoichiometry and nitrogen doping, Acs Sustain. Chem. Eng. 8 (14) (2020) 5566–5575.
[26] D. Qu, M. Zheng, L.G. Zhang, H.F. Zhao, Z.G. Xie, X.B. Jing, R.E. Haddad, H. Y. Fan, Z.C. Sun, Formation mechanism and optimization of highly luminescent N-doped graphene quantum dots, Sci. Rep. 4 (2014).
[27] B. Zhi, M.J. Gallagher, B.P. Frank, T.Y. Lyons, T.A. Qiu, J. Da, A.C. Mensch, R. J. Hamers, Z. Rosenzweig, D.H. Fairbrother, C.L. Haynes, Investigation of phosphorous doping effects on polymeric carbon dots: fluorescence, photostability, and environmental impact, Carbon 129 (2018) 438–449.
[28] B. Zhi, X.X. Yao, M. Wu, A. Mensch, Y. Cui, J.H. Deng, J.J. Duchimaza-Heredia, K. J. Trerayapiwat, T. Niehaus, Y. Nishimoto, B.P. Frank, Y.Q. Zhang, R.E. Lewis, E. A. Kappel, R.J. Hamers, H.D. Fairbrother, G. Orr, C.J. Murphy, Q. Cui, C. L. Haynes, Multicolor polymeric carbon dots: synthesis, separation and polyamide-supported molecular fluorescence, Chem. Sci. 12 (7) (2021) 2441–2455.
[29] Y.P. Sun, B. Zhou, Y. Lin, W. Wang, K.A.S. Fernando, P. Pathak, M.J. Meziani, B. A. Harruff, X. Wang, H.F. Wang, P.J.G. Luo, H. Yang, M.E. Kose, B.L. Chen, L. M. Veca, S.Y. Xie, Quantum-sized carbon dots for bright and colorful photoluminescence, J. Am. Chem. Soc. 128 (24) (2006) 7756–7757.
[30] H. Ding, J.S. Wei, P. Zhang, Z.Y. Zhou, Q.Y. Gao, H.M. Xiong, Solvent-Controlled synthesis of highly luminescent carbon dots with a wide color gamut and narrowed emission peak widths, Small 14 (22) (2018).
[31] M. Langer, T. Hrivnak, M. Medved, M. Otyepka, Contribution of the molecular fluorophore IPCA to excitation-independent photoluminescence of carbon dots, J. Phys. Chem. C 125 (22) (2021) 12140–12148.
[32] Y.F. Wang, Y.W. Zhu, S.M. Yu, C.L. Jiang, Fluorescent carbon dots: rational synthesis, tunable optical properties and analytical applications, RSC Adv. 7 (65) (2017) 40973–40989.
[33] T.H.T. Dang, V.T. Mai, Q.T. Le, N.H. Duong, X.D. Mai, Post-decorated surface fluorophores enhance the photoluminescence of carbon quantum dots, Chem. Phys. 527 (2019).
[34] W. Kasprzyk, P.P. Romanczyk, J. Feldmann, J.K. Stolarczyk, T. Swiergosz, The role of molecular fluorophores in the photoluminescence of carbon dots derived from citric acid: current state-of-the-art and future perspectives, Nanoscale 14 (39) (2022) 14368–14384.
[35] Y.M. Liu, P. Wang, K.A.S. Fernando, G.E. LeCroy, H. Maimaiti, B.A. Harruff-Miller, W.K. Lewis, C.E. Bunker, Z.L. Hou, Y.P. Sun, Enhanced fluorescence properties of carbon dots in polymer films, J. Mater. Chem. C 4 (29) (2016) 6967–6974.
[36] S. Chahal, J.R. Macairan, N. Yousefi, N. Tufenkji, R. Naccache, Green synthesis of carbon dots and their applications, RSC Adv. 11 (41) (2021) 25354–25363.
[37] H. Ding, X.H. Li, X.B. Chen, J.S. Wei, X.B. Li, H.M. Xiong, Surface states of carbon dots and their influences on luminescence, J. Appl. Phys. 127 (23) (2020).
[38] S.J. Zhu, Y.B. Song, X.H. Zhao, J.R. Shao, J.H. Zhang, B. Yang, The photoluminescence mechanism in carbon dots (graphene quantum dots, carbon nanodots, and polymer dots): current state and future perspective, Nano Res. 8 (2) (2015) 355–381.
[39] F. Ehrat, S. Bhattacharyya, J. Schneider, A. Löf, R. Wyrwich, A.L. Rogach, J. K. Stolarczyk, A.S. Urban, J. Feldmann, Tracking the source of carbon dot photoluminescence: aromatic domains versus molecular fluorophores, Nano Lett. 17 (12) (2017) 7710–7716.
[40] F.Y. Yan, Z.H. Sun, H. Zhang, X.D. Sun, Y.X. Jiang, Z.J. Bai, The fluorescence mechanismof carbon dots, and methods for tuning their emission color: a review, Microchim. Acta 186 (8) (2019).
[41] M. Langer, M. Paloncyova, M. Medved, M. Pykal, D. Nachtigallova, B.M. Shi, A.J. A. Aquino, H. Lischka, M. Otyepka, Progress and challenges in understanding of photoluminescence properties of carbon dots based on theoretical computations, Appl. Mater. Today 22 (2021).
[42] B. Zhi, X.X. Yao, Y. Cui, G. Orr, C.L. Haynes, Synthesis, applications and potential photoluminescence mechanism of spectrally tunable carbon dots, Nanoscale 11 (43) (2019) 20411–20428.
[43] M. Shamsipur, A. Barati, A.A. Taherpour, M. Jamshidi, Resolving the multiple emission centers in carbon dots: from fluorophore molecular states to aromatic domain states and carbon-core states, J. Phys. Chem. Lett. 9 (15) (2018) 4189–4198.
[44] L. Ai, Y.S. Yang, B.Y. Wang, J.B. Chang, Z.Y. Tang, B. Yang, S.Y. Lu, Insights into photoluminescence mechanisms of carbon dots: advances and perspectives, Sci. Bull. 66 (8) (2021) 839–856.
[45] F. Ehrat, S. Bhattacharyya, J. Schneider, A. Lof, R. Wyrwich, A.L. Rogach, J. K. Stolarczyk, A.S. Urban, J. Feldmann, Tracking the source of carbon dot photoluminescence: aromatic domains versus molecular fluorophores, Nano Lett. 17 (12) (2017) 7710–7716.
[46] N. Javed, D.M. O'Carroll, Carbon dots and stability of their optical properties, Part. Part. Syst. Char. 38 (4) (2021).
[47] A.V. Longo, A. Sciortino, M. Cannas, F. Messina, UV photobleaching of carbon nanodots investigated by in situ optical methods, Phys. Chem. Chem. Phys. 22 (24) (2020) 13398–13407.
[48] W. Kasprzyk, S. Bednarz, D. Bogdal, Luminescence phenomena of biodegradable photoluminescent poly(diol citrates), Chem. Commun. 49 (57) (2013) 6445–6447.
[49] W. Kasprzyk, S. Bednarz, P. Zmudzki, M. Galica, D. Bogdal, Novel efficient fluorophores synthesized from citric acid, RSC Adv. 5 (44) (2015) 34795–34799.
[50] W. Kasprzyk, T. Swiergosz, S. Bednarz, K. Walas, N.V. Bashmakova, D. Bogdal, Luminescence phenomena of carbon dots derived from citric acid and urea - a molecular insight, Nanoscale 10 (29) (2018) 13889–13894.
[51] S.J. Zhu, X.H. Zhao, Y.B. Song, S.Y. Lu, B. Yang, Beyond bottom-up carbon nanodots: citric-acid derived organic molecules, Nano Today 11 (2) (2016) 128–132.
[52] D. Qu, Z.C. Sun, The formation mechanism and fluorophores of carbon dots synthesized via a bottom-up route, Mater. Chem. Front. 4 (2) (2020) 400–420.
[53] Y. Li, C. Liu, H. Sun, M.L. Chen, D.F. Hou, Y.W. Zheng, H.J. Xie, B. Zhou, X. Lin, Formation and band gap tuning mechanism of multicolor emissive carbon dots from -hydroxybenzaldehyde, Adv. Sci. 10 (18) (2023).
[54] T. Lee, S. Won, Y. Park, W. Kwon, Oxygen-less carbon nanodots with an absolute quantum yield of 80% for display applications, ACS Appl. Nano Mater. 4 (3) (2021) 2462–2469.
[55] H.S. Shim, J. Choi, S. Jeong, S. Nam, J. Kim, J.K. Song, Fluorophore-dependent optical properties of multicolor carbon dots for bioimaging and optoelectronic devices, ACS Appl. Nano Mater. 6 (18) (2023) 17120–17129.
[56] H.S. Shim, J.M. Kim, S. Jeong, Y. Ju, S.J. Won, J. Choi, S. Nam, A. Molla, J. Kim, J.K. Song, Distinctive optical transitions of tunable multicolor carbon dots, Nanoscale Adv. 4 (5) (2022) 1351–1358.
[57] A. Hu, G. Chen, A. Huang, Z. Cai, T. Yang, C. Ma, L. Li, H. Gao, J. Gu, C. Zhu, Y. Wu, X. Qiu, J. Xu, J. Shen, L. Zhong, o-Phenylenediamine derived fluorescent carbon quantum dots for detection of Hg(II) in environmental water, J. Fluoresc. 34 (2) (2024) 905–913.
[58] Z.Y. Ding, F.F. Li, J.L. Wen, X.L. Wang, R.C. Sun, Gram-scale synthesis of single-crystalline graphene quantum dots derived from lignin biomass, Green Chem. 20 (6) (2018) 1383–1390.
[59] Y.B. Song, S.J. Zhu, S.T. Zhang, Y. Fu, L. Wang, X.H. Zhao, B. Yang, Investigation from chemical structure to photoluminescent mechanism: a type of carbon dots from the pyrolysis of citric acid and an amine, J. Mater. Chem. C 3 (23) (2015) 5976–5984.

[60] L. Shi, J.H. Yang, H.B. Zeng, Y.M. Chen, S.C. Yang, C. Wu, H. Zeng, O. Yoshihito, Q.Q. Zhang, Carbon dots with high fluorescence quantum yield: the fluorescence originates from organic fluorophores, Nanoscale 8 (30) (2016) 14374–14378.
[61] X.H. Liu, H.B. Li, L.J. Shi, X.R. Meng, Y.J. Wang, X. Chen, H. Xu, W.K. Zhang, X. M. Fang, T. Dinga, Structure and photoluminescence evolution of nanodots during pyrolysis of citric acid: from molecular nanoclusters to carbogenic nanoparticles, J. Mater. Chem. C 5 (39) (2017) 10302–10312.
[62] F. Siddique, M. Langer, M. Paloncyova, M. Medved, M. Otyepka, D. Nachtigallova, H. Lischka, A.J.A. Aquino, Conformational behavior and optical properties of a fluorophore dimer as a model of luminescent centers in carbon dots, J. Phys. Chem. C 124 (26) (2020) 14327–14337.
[63] E.V. Kundelev, E.D. Strievich, N.V. Tepliakov, A.D. Murkina, A.Y. Dubavik, E. V. Ushakova, A.V. Baranov, A.V. Fedorov, I.D. Rukhlenko, A.L. Rogach, Structure-optical property relationship of carbon dots with molecular-like blue-emitting centers, J. Phys. Chem. C 126 (42) (2022) 18170–18176.
[64] M. Langer, M. Paloncyova, M. Medveď, M. Otyepka, Molecular fluorophores self-organize into C-dot seeds and incorporate into C-dot structures, J. Phys. Chem. Lett. 11 (19) (2020) 8252–8258.
[65] A. Diaspro, G. Chirico, C. Usai, P. Ramoino, J. Dobrucki, Photobleaching, in: J. B. Pawley (Ed.), Handbook of Biological Confocal Microscopy, Springer US, Boston, MA, 2006, pp. 690–702.
[66] D.Y. Jin, P. Xi, B.M. Wang, L. Zhang, J. Enderlein, A.M. van Oijen, Nanoparticles for super-resolution microscopy and single-molecule tracking, Nat. Methods 15 (6) (2018) 415–423.
[67] Y. Xiong, J. Schneider, C.J. Reckmeier, H. Huang, P. Kasak, A.L. Rogach, Carbonization conditions influence the emission characteristics and the stability against photobleaching of nitrogen doped carbon dots, Nanoscale 9 (32) (2017) 11730–11738.
[68] B.P. Frank, L.R. Sigmon, A.R. Deline, R.S. Lankone, M.J. Gallagher, B. Zhi, C. L. Haynes, D.H. Fairbrother, Photochemical transformations of carbon dots in aqueous environments, Environ. Sci. Technol. 54 (7) (2020) 4160–4170.
[69] W.S. Wang, C. Damm, J. Walter, T.J. Nacken, W. Peukert, Photobleaching and stabilization of carbon nanodots produced by solvothermal synthesis, Phys. Chem. Chem. Phys. 18 (1) (2016) 466–475.
[70] A. Terracina, A. Armano, M. Meloni, A. Panniello, G. Minervini, A. Madonia, M. Cannas, M. Striccoli, L. Malfatti, F. Messina, Photobleaching and recovery kinetics of a palette of carbon nanodots probed by in situ optical spectroscopy, ACS Appl. Mater. Interfaces (2022).
[71] L. Cao, M.H. Zan, F.M. Chen, X.Y. Kou, Y.L. Liu, P.Y. Wang, Q. Mei, Z. Hou, W. F. Dong, L. Li, Formation mechanism of carbon dots: from chemical structures to fluorescent behaviors, Carbon 194 (2022) 42–51.
[72] B.C. Han, X. Hu, X.F. Zhang, X.J. Huang, M.Z. An, X. Chen, D. Zhao, J. Li, The fluorescence mechanism of carbon dots based on the separation and identification of small molecular fluorophores, RSC Adv. 12 (19) (2022) 11640–11648.
[73] V. Strauss, H.Z. Wang, S. Delacroix, M. Ledendecker, P. Wessig, Carbon nanodots revised: the thermal citric acid/urea reaction, Chem. Sci. 11 (31) (2020) 8256–8266.
[74] A. Philippidis, A. Spyros, D. Anglos, A.B. Bourlinos, R. Zboril, E.P. Giannelis, Carbon-dot organic surface modifier analysis by solution-state NMR spectroscopy, J. Nanoparticle Res. 15 (7) (2013).
[75] F. Yang, G.E. LeCroy, P. Wang, W.X. Liang, J.J. Chen, K.A.S. Fernando, C. E. Bunker, H.J. Qian, Y.P. Sun, Functionalization of carbon nanoparticles and defunctionalization-toward structural and mechanistic elucidation of carbon "quantum" dots, J. Phys. Chem. C 120 (44) (2016) 25604–25611.
[76] G.E. LeCroy, S.K. Sonkar, F. Yang, L.M. Veca, P. Wang, K.N. Tackett, J.J. Yu, E. Vasile, H.J. Qian, Y.M. Liu, P. Luo, Y.P. Sun, Toward structurally defined carbon dots as ultracompact fluorescent probes, ACS Nano 8 (5) (2014) 4522–4529.
[77] P. Devi, A. Thakur, S. Chopra, N. Kaur, P. Kumar, N. Singh, M. Kumar, S. M. Shivaprasad, M.K. Nayak, Ultrasensitive and selective sensing of selenium using nitrogen-rich ligand interfaced carbon quantum dots, ACS Appl. Mater. Interfaces 9 (15) (2017) 13448–13456.
[78] S. Cailotto, E. Amadio, M. Facchin, M. Selva, E. Pontoglio, F. Rizzolio, P. Riello, G. Toffoli, A. Benedetti, A. Perosa, Carbon dots from sugars and ascorbic acid: role of the precursors on morphology, properties, toxicity, and drug uptake, ACS Med. Chem. Lett. 9 (8) (2018) 832–837.
[79] S. Cailotto, R. Mazzaro, F. Enrichi, A. Vomiero, M. Selva, E. Cattaruzza, D. Cristofori, E. Amadio, A. Perosa, Design of carbon dots for metal-free photoredox catalysis, ACS Appl. Mater. Interfaces 10 (47) (2018) 40560–40567.
[80] L. Vallan, E.P. Urriolabeitia, F. Ruiperez, J.M. Matxain, R. Canton-Vitoria, N. Tagmatarchis, A.M. Benito, W.K. Maser, Supramolecular-enhanced charge transfer within entangled polyamide chains as the origin of the universal blue fluorescence of polymer carbon dots, J. Am. Chem. Soc. 140 (40) (2018) 12862–12869.
[81] J.M. Arroyave, R.E. Ambrusi, Y. Robein, M.E. Pronsato, G. Brizuela, M.S. Di Nezio, M.E. Centuri, Carbon dots structural characterization by solution-state NMR and UV-visible spectroscopy and DFT modeling, Appl. Surf. Sci. 564 (2021).
[82] K. Bramhaiah, R. Bhuyan, S. Mandal, S. Kar, R. Prabhu, N.S. John, M. Gramlich, A.S. Urban, S. Bhattacharyya, Molecular, aromatic, and amorphous domains of N-carbon dots: leading toward the competitive photoluminescence and photocatalytic properties, J. Phys. Chem. C 125 (7) (2021) 4299–4309.
[83] A.A. Kokorina, A.V. Sapelkin, G.B. Sukhorukov, I.Y. Goryachev, Luminescent carbon nanoparticles separation and purification, Adv. Colloid Interface Sci. 274 (2019).
[84] S.N. Yang, Y.M. Zhang, Y.Y. Xue, S.J. Lu, H.Y. Yang, L. Yang, C.F. Ding, S.N. Yu, Cross-linked polyamide chains enhanced the fluorescence of polymer carbon dots, ACS Omega 5 (14) (2020) 8219–8229.
[85] K.J. Mintz, M. Bartoli, M. Rovere, Y.Q. Zhou, S.D. Hettiarachchi, S. Paudyal, J. Y. Chen, J.B. Domena, P.Y. Liyanage, R. Sampson, D. Khadka, R.R. Pandey, S. X. Huang, C.C. Chusuei, A. Tagliaferro, R.M. Leblanc, A deep investigation into the structure of carbon dots, Carbon 173 (2021) 433–447.
[86] B. Bartolomei, A. Bogo, F. Amato, G. Ragazzon, M. Prato, Nuclear magnetic resonance reveals molecular species in carbon nanodot samples disclosing flaws, Angew. Chem. Int. Ed. 61 (20) (2022).
[87] A. Das, V. Gude, D. Roy, T. Chatterjee, C.K. De, P.K. Mandal, On the molecular origin of photoluminescence of nonblinking carbon dot, J. Phys. Chem. C 121 (17) (2017) 9634–9641.
[88] M. Rougee, R.V. Bensasson, E.J. Land, R. Pariente, Deactivation of singlet molecular oxygen by thiols and related compounds, possible protectors against SKIN photosensitivity, Photochem. Photobiol. 47 (4) (1988) 485–489.
[89] A.T.R. Williams, S.A. Winfield, J.N. Miller, Relative fluorescence quantum yields using a computer-controlled luminescence spectrometer, Analyst 108 (1290) (1983) 1067–1071.
[90] A.M. Brouwer, Standards for photoluminescence quantum yield measurements in solution, IUPAC Tech. Rep. 83 (12) (2011) 2213–2228.
[91] E. Mordovina, A. Bakal, D. Tsyupka, A. Vostrikova, V. Olomskaya, I. Y. Goryacheva, Factors Affecting Photoluminescence of Structures Based on Citric Acid and Ethylenediamine, vol. 11065, SPIE, 2019.
[92] J.C. Kung, I.T. Tseng, C.S. Chien, S.H. Lin, C.C. Wang, C.J. Shih, Microwave assisted synthesis of negative-charge carbon dots with potential antibacterial activity against multi-drug resistant bacteria, RSC Adv. 10 (67) (2020) 41202–41208.
[93] J. Schneider, C.J. Reckmeier, Y. Xiong, M. von Seckendorff, A.S. Susha, P. Kasak, A.L. Rogach, Molecular fluorescence in citric acid-based carbon dots, J. Phys. Chem. C 121 (3) (2017) 2014–2022.
[94] X.Y. Zhai, P. Zhang, C.J. Liu, T. Bai, W.C. Li, L.M. Dai, W.G. Liu, Highly luminescent carbon nanodots by microwave-assisted pyrolysis, Chem. Commun. 48 (64) (2012) 7955–7957.
[95] F. Meierhofer, F. Dissinger, F. Weigert, J. Jungclaus, K. Muller-Caspary, S. R. Waldvogel, U. Resch-Genger, T. Voss, Citric acid based carbon dots with amine type stabilizers: pH-specific luminescence and quantum yield characteristics, J. Phys. Chem. C 124 (16) (2020) 8894–8904.
[96] P. Duan, B. Zhi, L. Coburn, C.L. Haynes, K. Schmidt-Rohr, A molecular fluorophore in citric acid/ethylenediamine carbon dots identified and quantified by multinuclear solid-state nuclear magnetic resonance, Magn. Reson. Chem. 58 (11) (2020) 1130–1138.
[97] L. Dordevic, F. Arcudi, M. Cacioppo, M. Prato, A multifunctional chemical toolbox to engineer carbon dots for biomedical and energy applications, Nat. Nanotechnol. 17 (2) (2022) 112–130.
[98] F.M.a. d.D. Dayrit, C. Angel, 1H and 13C NMR for the profiling of natural product extracts: theory and applications, in: F.Z. Eram Sharmin (Ed.), Spectroscopic Analyses, IntechOpen, Rijeka, Croatia, 2017.
[99] M. Wu, A.M. Vartanian, G.N. Chong, A.K. Pandiakumar, R.J. Hamers, R. Hernandez, C.J. Murphy, Solution NMR analysis of ligand environment in quaternary ammonium-terminated self -assembled monolayers on gold nanoparticles: the effect of surface curvature and ligand structure, J. Am. Chem. Soc. 141 (10) (2019) 4316–4327.
[100] M. Usman, Y. Zaheer, M.R. Younis, R.E. Demirdogen, S.Z. Hussain, Y. Sarwar, M. Rehman, W.S. Khan, A. Ihsan, The effect of surface charge on cellular uptake and inflammatory behavior of carbon dots, Colloid Interface Sci. Commun. 35 (2020).
[101] N. Dhenadhayalan, K.C. Lin, Chemically induced fluorescence switching of carbon-dots and its multiple logic gate implementation, Sci. Rep. 5 (2015).
[102] J.K. Yu, X. Yong, Z.Y. Tang, B. Yang, S.Y. Lu, Theoretical understanding of structure-property relationships in luminescence of carbon dots, J. Phys. Chem. Lett. 12 (32) (2021) 7671–7687.
[103] X.M. Wen, P. Yu, Y.R. Toh, X.T. Hao, J. Tang, Intrinsic and extrinsic fluorescence in carbon nanodots: ultrafast time-resolved fluorescence and carrier dynamics, Adv. Opt. Mater. 1 (2) (2013) 173–178.
[104] M.J. Krysmann, A. Kelarakis, P. Dallas, E.P. Giannelis, Formation mechanism of carbogenic nanoparticles with dual photoluminescence emission, J. Am. Chem. Soc. 134 (2) (2012) 747–750.
[105] Sigmon, L. R.; Catazaro, J.; Fairbrother, D. H., Structure of Carbon Dots Elucidated by Solution Phase NMR. **Manuscript in Preparation**.
[106] R. Novoa-Carballal, M. Martin-Pastor, E. Fernandez-Megia, Unveiling an NMR-invisible fraction of polymers in solution by saturation transfer difference, ACS Macro Lett. 10 (12) (2021) 1474–1479.
[107] C.M. Carbonaro, R. Corpino, M. Salis, F. Mocci, S.V. Thakkar, C. Olla, P.C. Ricci, On the emission properties of carbon dots: reviewing data and discussing models, C-J. Carbon Res. 5 (4) (2019).
[108] X. Chen, G. Fang, C. Liu, D.D. Dionysiou, X. Wang, C. Zhu, Y. Wang, J. Gao, D. Zhou, Cotransformation of carbon dots and contaminant under light in aqueous solutions: a mechanistic study, Environ. Sci. Technol. 53 (11) (2019) 6235–6244.
[109] Y. Gong, B. Yu, W. Yang, X. Zhang, Phosphorus, and nitrogen co-doped carbon dots as a fluorescent probe for real-time measurement of reactive oxygen and nitrogen species inside macrophages, Biosens. Bioelectron. 79 (2016) 822–828.
[110] A. Cappai, C. Melis, L. Stagi, P.C. Ricci, F. Mocci, C.M. Carbonaro, Insight into the molecular model in carbon dots through experimental and theoretical analysis of citrazinic acid in aqueous solution, J. Phys. Chem. C 125 (8) (2021) 4836–4845.

[111] F. Mocci, C. Olla, A. Cappai, R. Corpino, P.C. Ricci, D. Chiriu, M. Salis, C. M. Carbonaro, Formation of citrazinic acid ions and their contribution to optical and magnetic features of carbon nanodots: a combined experimental and computational approach, Materials 14 (4) (2021).
[112] S. Mura, L. Stagi, L. Malfatti, C.M. Carbonaro, R. Ludmerczki, P. Innocenzi, Modulating the optical properties of citrazinic acid through the monomer-to-dimer transformation, J. Phys. Chem. A 124 (1) (2020) 197–203.
[113] L. Stagi, S. Mura, L. Malfatti, C.M. Carbonaro, P.C. Ricci, S. Porcu, F. Secci, P. Innocenzi, Anomalous optical properties of citrazinic acid under extreme pH conditions, ACS Omega 5 (19) (2020) 10958–10964.
[114] W. Wang, B. Wang, H. Embrechts, C. Damm, A. Cadranel, V. Strauss, M. Distaso, V. Hinterberger, D.M. Guldi, W. Peukert, Shedding light on the effective fluorophore structure of high fluorescence quantum yield carbon nanodots, RSC Adv. 7 (40) (2017) 24771–24780.
[115] S. Benz, S. Notzli, J.S. Siegel, D. Eberli, H.J. Jessen, Controlled oxygen release from pyridone endoperoxides promotes cell survival under anoxic conditions, J. Med. Chem. 56 (24) (2013) 10171–10182.
[116] N. Zeinali, I. Oluwoye, M. Altarawneh, B.Z. Dlugogorski, The mechanism of electrophilic addition of singlet oxygen to pyrrolic ring, Theor. Chem. Acc. 138 (7) (2019).